International Journal of Engineering & Technology, 7 (4) (2018) 2332-2337

International Journal of Engineering & Technology

Website: www.sciencepubco.com/index.php/IJET
doi: 10.14419/ijet.v7i4.10771
Research paper

Temperature distribution of T- joint friction stir welding

Sadiq Aziz Hussein [1] *, Shaymaa Abdul Khader Al-Jumaili [2], Raed A. Mahmood [2]

[1] Technical Instructors Training Institute, Middle Technical University, Baghdad, Iraq
[2] Almussaib Technical College, Alfurat Alawsat Technical University, 51009 Babel, Iraq.
**Corresponding author E-mail: sadiq@mtu.edu.iq*

Abstract

Friction stir welding is a reliable welding method; it can be employed to join different structural configurations. Joint types such as lap, butt and T have been successfully produced by this welding method. In this study, a trial has been made to numerically simulate the heat generation and temperature distribution during the welding process of a T-joint. The workpieces materials were hardened 5052 and tempered 7075 Al Alloys, each material was investigated separately. Different rotational and welding speeds were used, besides, the pin length was also varied to accommodate the investigation of the top plate thickness effect. A visco-plastic finite element model was adopted to investigate the effect of parameters ranges on the temperature distribution. The results showed that the temperature distribution of T-joint depends mainly on the material to be welded and rotational speed. Besides, increasing the pin length from 7 to 10 mm could significantly increase the resulted temperature by approximately 14%. Therefore, the thickness of the upper plates of the T-joint plays a significant role on the resulted process temperature.

Keywords: *FSW; T-Joint; AA5052; AA7075; Temperature Distribution; Peak Temperature.*

1. Introduction

Friction Stir Welding (FSW) is a thermos-mechanical solid-state welding method. It is environmentally friendly, and therefore, this technique attracted much attention and development during the last three decades. Many applications which manufactured by using FSW are reported in the literature [1], [2]. The joints of these applications are made from similar or dissimilar materials and the structure could be in a butt and/or a lap configuration. Recently, the T-joint has been made by this welding method as well [3]. In general, the main input and output factors of the FSW method can be explained as shown in Figure 1.

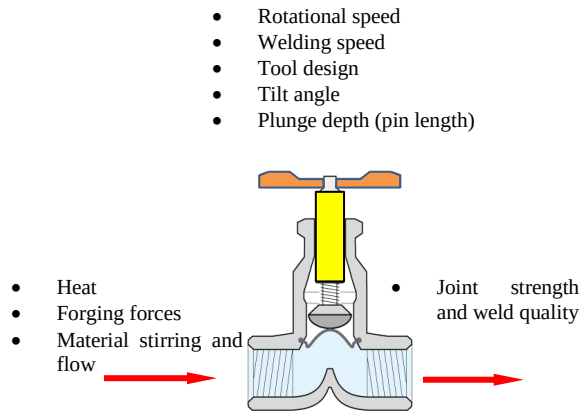


Fig. 1: The Main Affected Parameters of the Friction Stir Welding.

T-joints cannot be recompense in many structural parts of shipbuilding, automotive and aerospace applications. The T-joint are widely used to join skin-to-stringer (stiffeners) components of such structure. However, the associated defects are the challenging issue that faces such joint configuration. In general, insufficient material flow and heat input lead to abnormal stirring and hence the promotion of such defects. Cui et al. [4] have described the difficulty of producing a high-quality T-joint weld by FSW due to the various defect formation. The welding parameters (rotational and welding speeds) are the main affected factors. Zhao et al. [5] refer to the tunnel defects that usually formed at the advancing side of the weld adjacent to the contact surface between the skin and the stringer, which occurred due to the poor material flow. They reported that increasing the weld pitch (rotational speed to the welding speed) could reduce the formation and size of such defects. Another defect type "kissing bond" was extended through the weld line as well. Besides, the geometry of the tool and the joint demonstrate a considerable influence on these formation defects [6]. To eliminate the defect of T-joint Jesus et al. [7] examined three different tools. For example, different defects were noticed within the joint zone which produced by using a pyramidal pin tool while the welds produced with a tapered pin tool resulted in less defect formation. However, the welds made by a progressive tool did not show defects.

Tool rotational and traveling speeds are the dominated parameters on the material flow and associated heat, and so, defect formation incidents as indicated by Podržaj et al. [8]. Therefore, it is very important to understand the heat generation process, temperature distribution and resulted peak temperature before implementing any experimental work for T-joint. Very few publications to investigate the heat generation and temperature distribution are available in the literature concerning the T-joint configuration. Therefore, the present work is to evaluate the temperature distribution of different materials arranged in this joint type. The study used a visco-plastic model to validate the aimed heat generation process and related process temperature.

Nomenclature

P; Pressure of the plastic flow.
Z; Zener-Hollomon parameter.

Copyright © 2018 Sadiq Aziz Hussein et. al. This is an open access article distributed under the Creative Commons Attribution License, which permits unrestricted use, distribution, and reproduction in any medium, provided the original work is properly cited.

A; Reciprocal strain factor.
Q; Temperature independent activation energy.
R; Universal gas constant.
N; Rotational speed.
V; welding speed.
PH; Pin height.
T_p; Peak temperature.
U; Plastic flow velocity.
P; Density.
μ; Dynamic viscosity.
V; Travel velocity.
σ_e; Flow stress.
A and n Material constants.
$\dot{\varepsilon}$; Effective strain rate.
C_P; Specific heat.
K; Thermal conductivity.

2. Description of the model

In the present work, the modeling was implemented through Altair HyperWorks™ software. This relatively new software is developed by Altair Engineering. HyperWorks has been efficiently employed in many research sectors and manufacturing solutions. Lately, some studies implement this software for the FSW simulation [9-10]. Many other finite element software were used to determine the temperature distribution and T_p during the FSW process [11]. The mass flow of material was assumed to act as incompressible non-Newtonian and visco-plastic, such assumption is agreed by many other studies [12]. The continuity equation for incompressible single-phase flow is explained as explained in Equation (1). The index notation of i is equal to 1, 2, and 3, this indexing representing x, y, and z directions, respectively [12].

$$\frac{\partial u_i}{\partial x_i} = 0 \tag{1}$$

$$\rho \frac{\partial u_i u_j}{\partial x_i} = -\frac{\partial P}{\partial x_j} + \frac{\partial}{\partial x_i}\left(\mu \frac{\partial u_j}{\partial x_i} + \mu \frac{\partial u_i}{\partial x_j}\right) - \rho v \frac{\partial u_i}{\partial u_j} \tag{2}$$

The viscosity is carefully measured based on the next flow stress formulation [12]

$$\sigma_e = \frac{1}{\alpha} \sinh^{-1}\left[\left(\frac{Z}{A}\right)^{\frac{1}{n}}\right] \tag{3}$$

Where

$$Z = \dot{\varepsilon} \exp\left(\frac{Q}{RT}\right) \tag{4}$$

$$\dot{\varepsilon} = \left(\frac{2}{3} \varepsilon_{ij} \varepsilon_{ij}\right)^{1/2} \tag{5}$$

While the effective strain rate and the stress flow which can be used to determine the viscosity can be computed as follow:

$$\mu = \frac{\sigma_e}{3\dot{\varepsilon}} \tag{6}$$

The values of thermal properties and the other constants are shown in Table 1.

Table 1: The Thermal Properties and Other Constants of the Numerical Model

Property	AA5052	AA7075
ρ (Kg/m^3)	2680	2810
c_p (J/Kg.K)	880	960
k (W/m.K)	137	173
Coeff. of thermal Expan. (1/K)	1e-005	1e-005
Stress exponent	5.24	5.41
A (1/sec)	4.23824 e+10	1.02709 e+09
α (1/MPa)	0.016	0.0141
Q (J/mol)	155167	129400
R (J/mol.K)	8.314	8.314

3D Hexahedral with 20 nodes was the carefully chosen element. The element serves 3 degrees of freedom for both mechanical and thermal analysis. Figure 2 shows the schematic of the model and its dimensions while the developed model at final mesh configuration is shown in Figure 3. The Galerkin's weighted residual method was used to obtain the strain calculation. The relation between strain rate, flow stress and viscosity of both AA5052 and AA7075 are shown in Figures 4 and 5, respectively.

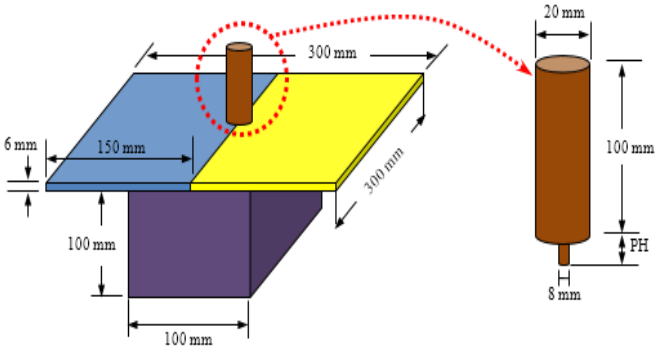


Fig. 2: The Dimensions of FSW Model.

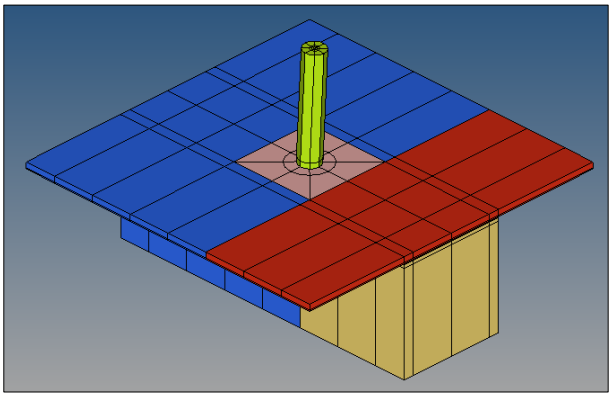


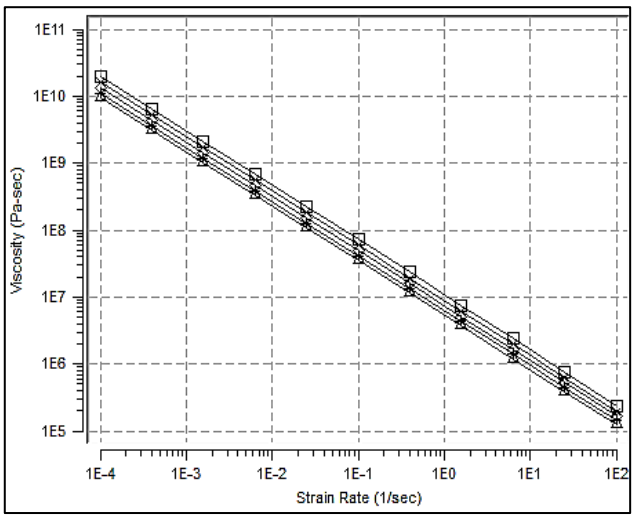
Fig. 3: Schematic Diagram of the Numerical Model and the Mesh.

The rotational and welding speeds along with penetration depth are the main technological welding process parameters [13]. The parameters for investigation in this study were as shown in Table 2.

Table 2: The Welding Process Parameters and the Investigated Range

Welding parameters	value
N (rpm)	400, 500, 600
v (mm/s)	2, 4
PH (mm)	7, 8.5, 10
Tilt angle (deg)	3

(A)



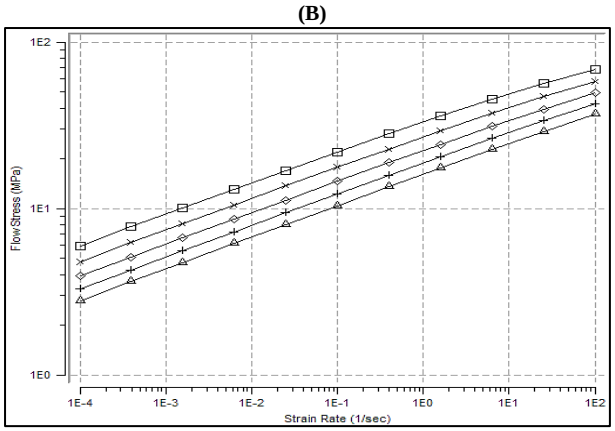


Fig. 4: Relation between Strain Rate of AA5052 for Various Temperatures with (A) Viscosity and (B) Flow Stress [14].

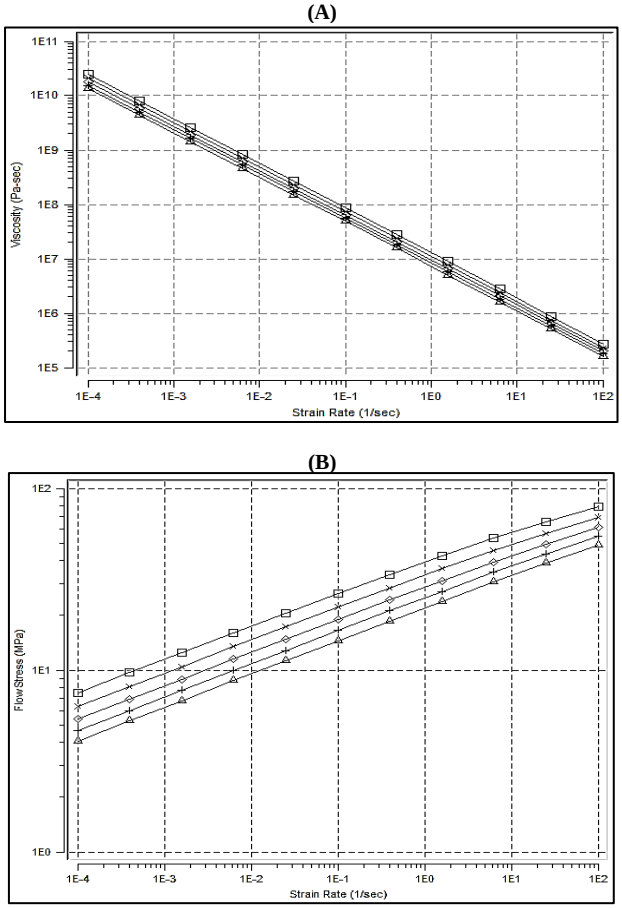


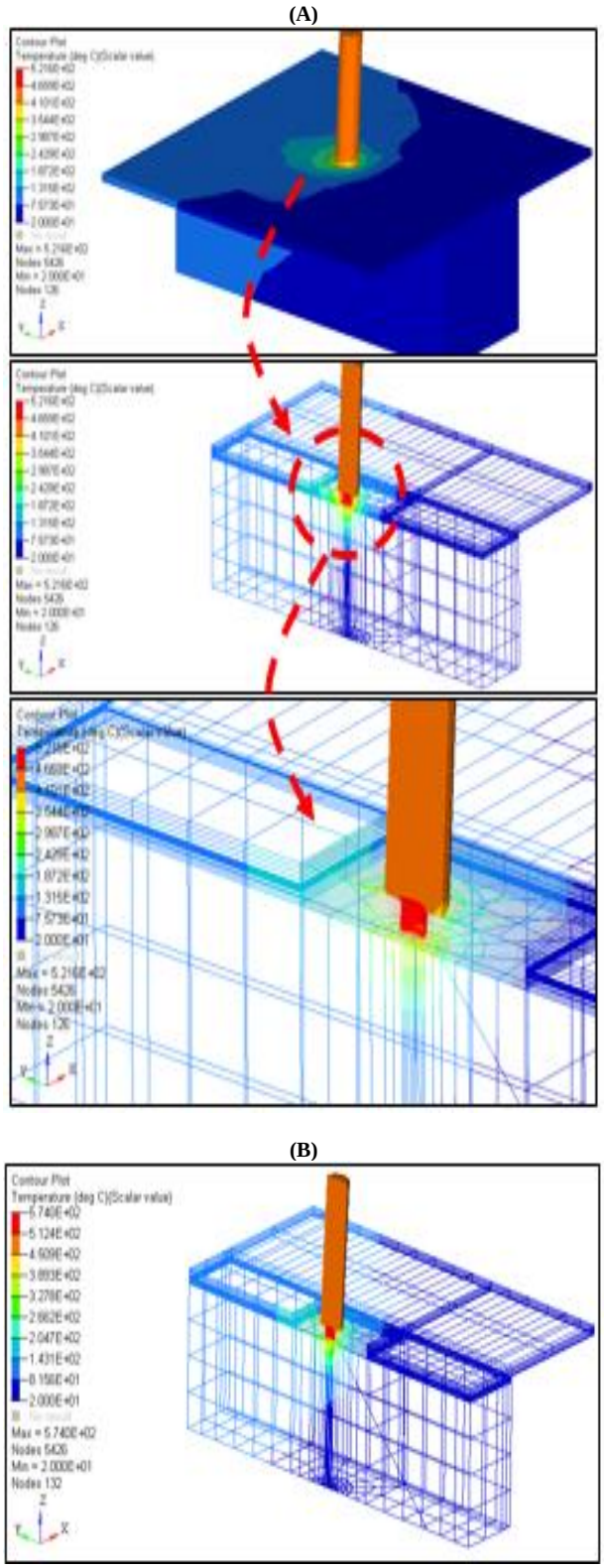
Fig. 5: Relation between Strain Rate of AA7075 for Various Temperatures with (A) Viscosity and (B) Flow Stress [14].

3. Results and discussion

The first sight of the model contour results showed that the peak temperature of the welding process was significantly influenced by the tool geometry (pin height) and main welding parameters as well as the characteristics of the material being welded. Therefore, the analysis of each parameter effect on the resulted heat is presented separately.

3.1. Effect of rotational speed

The rotational speed can be assumed as the superior affected parameters on the generated heat in the most literature [1], [15]. For constant welding speed, high tool rotational speed produces large heat input, which mainly resulted from the severe plastic flow of the material [16]. In the present study, T_p was 522 °C when N = 400 rpm and 574 °C when N = 500 rpm for the same v and PH. The increment ratio of T_p was approximately 9% while it was 15% when the N increased to 600 rpm. Figure 6 shows the contour plot of the model affected by the changing of the rotational speed values. It is worth to notice that the temperature distribution showed widen profile of the high temperature distribution especially when high rotational speed together with slow welding speed were used. The maximum presence of T_p was closed to the pin zone at the stir material area due to the plastic deformation incident. Such results agreed the relevant works so far [12], [16], [17]. It is important to notice that the contour plot of the temperature distribution at the bottom plate is generally similar to that of the upper plates.



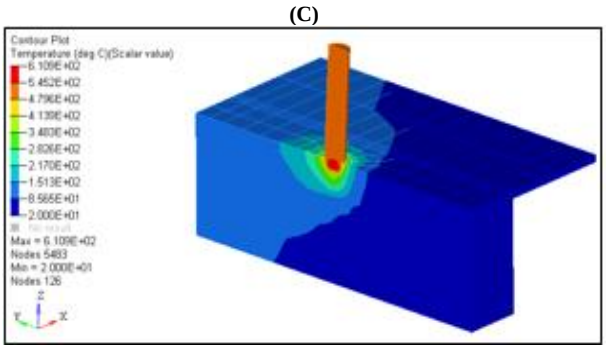
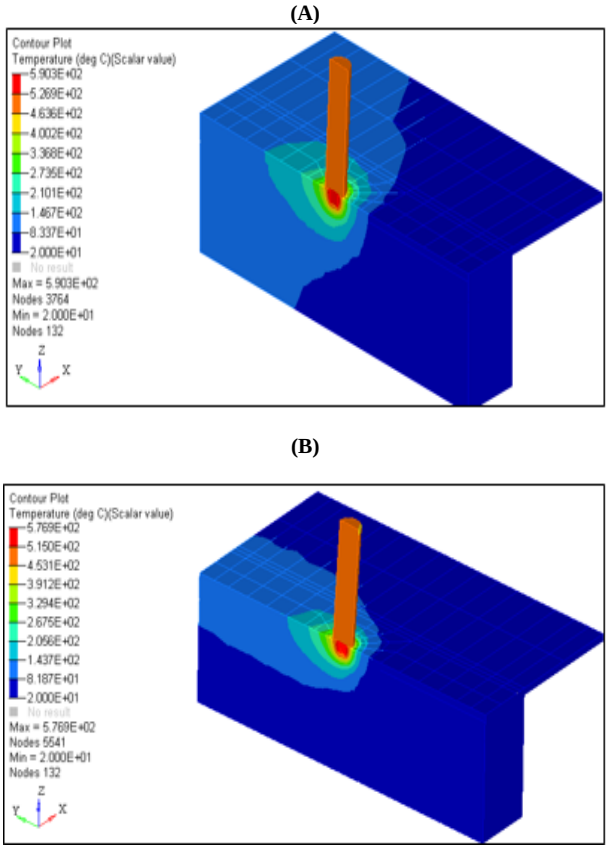


Fig. 6: Effect of Rotational Speed Parameter on the Resulted Peak Temperature of AA7075 Material (A) N = 400 rpm, PH = 7 mm, and V = 2 mm/S (B) N = 500 rpm, PH = 7 mm, and V = 2 mm/S (C) N = 600 rpm, PH= 7 mm, and V = 2 mm/S.

3.2. Effect of welding speed

It is well known that the rotation of the tool caused materials stirring around the tool pin whereas the movement of the tool relocations this stirred material aggressively from the front to the back of the pin. Liu et al. [18] stated that material deformation and the heat input incident would be low when welding speed is reduced during the FSW process for the same value of rotational speed. Hou et al. [19] agreed this fact, besides; they stated that the softening region is most likely to narrow down with an increase in the welding speed. It is evident that similar results were obtained for the T-joint of this study concerning the lower heat and narrow affected area by the high temperature profiles. This can be attributed to the shorter staying time of welding tool at each point along the welding line when faster welding speed has been used. Figure 7 explains the intended results, the slightly decrease in T_p value is clear through the temperature contour plot. When N was constant at 400 rpm and PH was 10 mm, the T_p decreased by 2% if v increased from 2 mm/s to 4 mm/s. Similar percent of reduction was obtained when N was 600 rpm for same other condition.



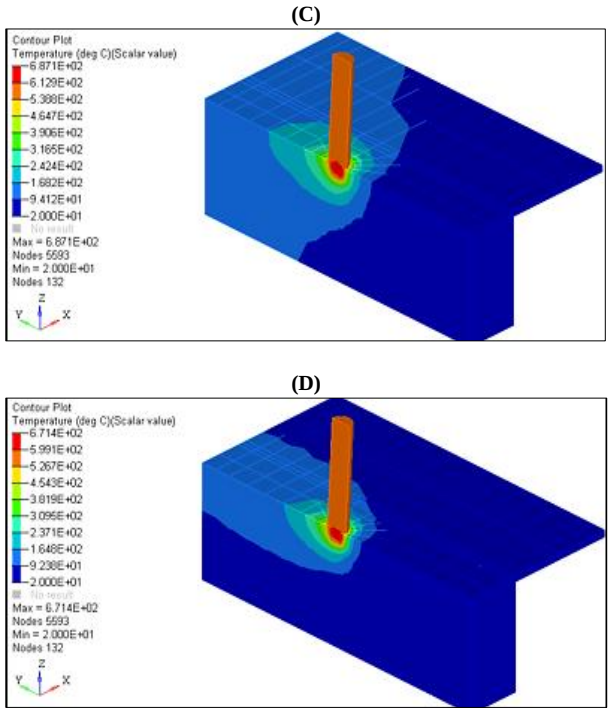
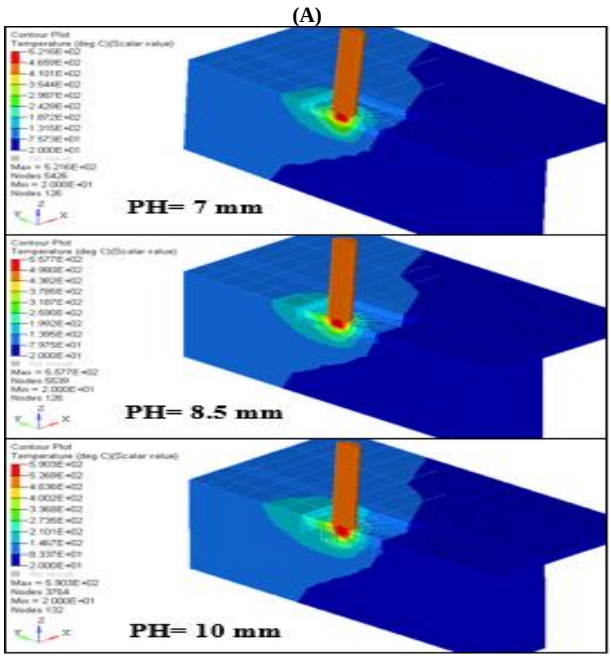


Fig. 7: The Effect of Welding Speed Parameter on the Resulted Peak Temperature of AA7075 Material (A) N = 400 rpm, PH = 10 mm, and V = 2 mm/S (B) N = 400 rpm, PH = 10 mm, and V = 4 mm/S (C) N = 600 rpm, PH= 10 mm, and V = 2 mm/S, (D) N = 600 rpm, PH= 10 mm, and V = 4 mm/S.

3.3. Effect of pin length

As mentioned by Fratini et al [20], the tool pin is strongly decided the in-situ material flow during the FSW process. Figure 8 Explains the results of the PH factor effect on the temperature profiles for different rotational and welding speeds. The maximum temperature zone seems to be extended at the surrounded outer surface of the pin. When PH increased from 7 mm to 10 mm, the T_p increased by 13% and 12 % for N 400 rpm and 600 rpm, respectively, while v kept constant. The effect of PH is explained clearly in Figure 9 for three different values and for various N and v. However, the pin length role on the generated heat was increased when the material to be welded was AA5052 as it will be explained later.



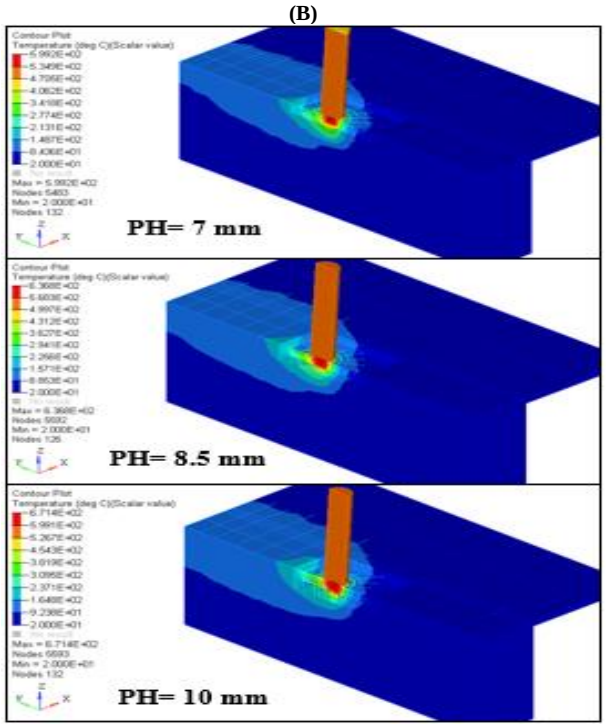
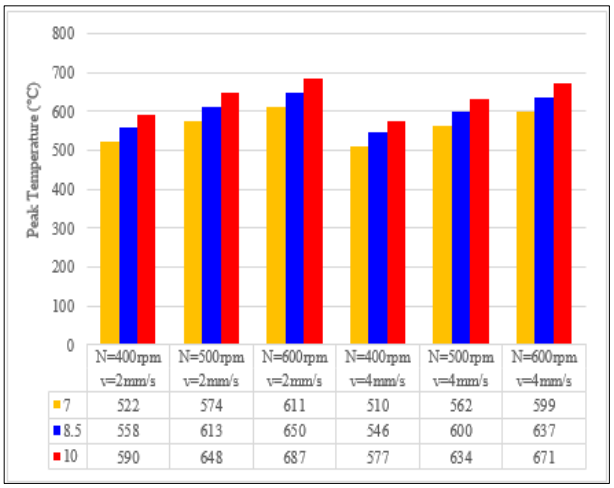


Fig. 8: The Pin Length Effect on the Resulted Peak Temperature of AA7075 for Different Rotational and Welding Speeds (A) N = 400 rpm, V = 2 mm/S (B) N = 600 rpm, V = 4 mm/S.



	N=400rpm v=2mm/s	N=500rpm v=2mm/s	N=600rpm v=2mm/s	N=400rpm v=4mm/s	N=500rpm v=4mm/s	N=600rpm v=4mm/s
7	522	574	611	510	562	599
8.5	558	613	650	546	600	637
10	590	648	687	577	634	671

Fig. 9: The Effect of Pin Length on the Resulted Peak Temperature of AA7075 for Different Welding Parameters.

3.4. Material effect

The material dependent, thermal and plastic properties affect the resulted T_p value of the present model. When the material changed from AA7075 to the work hardened Al Alloy (AA5052), the increment of T_p was approximately 5.5% for same welding parameters. The other parameters were investigated for the AA5052 material. It was found that the more significant affected parameter was the rotational speed which resulted in 18.9% increment when N increased from 400 rpm to 600 rpm as shown in Figure 10. The increment percent was 14.3% when the tool PH was elongated from [7] to 10 mm. On the other side, increasing v to 4mm/s decreased the T_p by 1.8%. In general, the difference in T_p between the two investigated Al Alloys is depicted in Figure 11 for constant welding parameters. In general, the resulted temperature of the aimed joint (T-joint) concerning the temperature profile is similar foremost to that observed in other joint configurations. Notably, the temperature profile at the bottom plate of the T-joint showed similar temperature contour of that at each side of butt joint. Among the selected parameter and their values to be investigated in this study, the N and PH showed the more significant effects. They are the most relevant process variables that determining the mainly thermal contribution conferred to the T-joint. Besides, welding of work-hardened Al Alloys lead to high T_p, this can be related to the difference in strain rate, the flow of stress and viscosity of both materials. The other properties shown in Table 1 could also significantly contributed to such material effect on the resulted temperature.

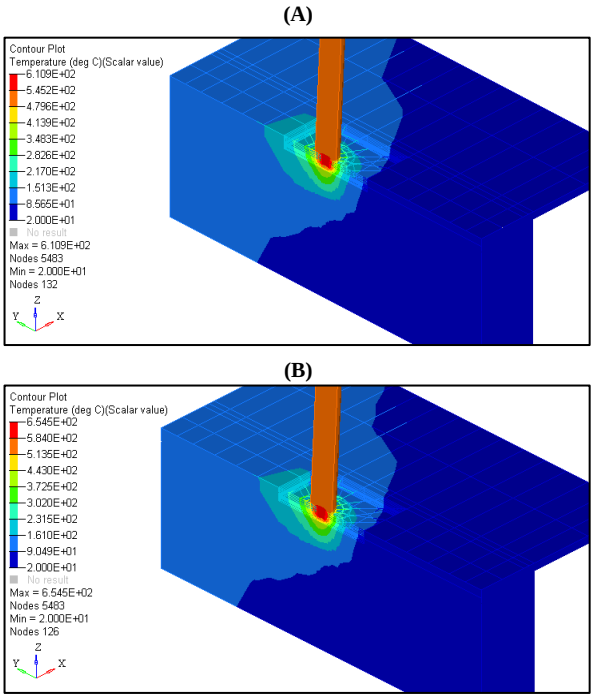
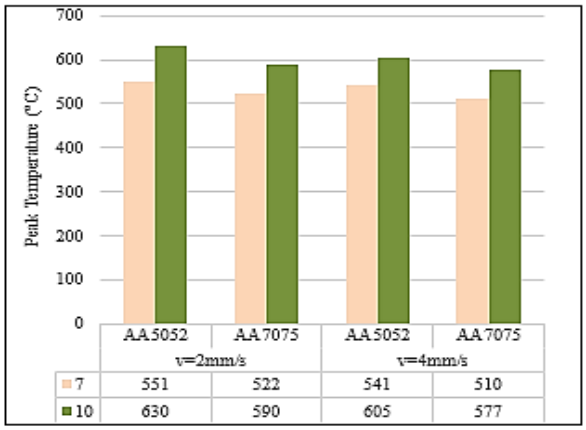


Figure 10: The Material Effect on the Resulted Temperature Profile for the Same Welding Parameters, (A) AA7075 and (B) AA5052.



	AA5052 v=2mm/s	AA7075 v=2mm/s	AA5052 v=4mm/s	AA7075 v=4mm/s
7	551	522	541	510
10	630	590	605	577

Figure 11: The Difference in T_p Values of the Two Investigated Al Alloys for Constant Welding Parameters.

4. Conclusion

In the present work, the results of numerical investigations on FSW of T-joints are included for two different Al Alloys, namely the AA5052 and AA7075 grades. It is found that the two considered materials denote a considerably different resulted temperature. It can be concluded that AA5052 is definitively producing higher peak temperature than AA7075 of the present model. The rotational and pin depth were the most significant parameters on the resulted heat. The increment ratio can attain approximately 19% when rotational speed increased by 200 rpm. The temperature profile at the upper two plates of the T-joint was generally similar to that of the butt joint. However, the temperature contour at the bottom plate exposed similar profile to those (upper) plates along its height. The pin length should be carefully selected to avoid the undesired high

temperature while the need of increasing the peak temperature imply the long pin height. For example, when the pin length increased by 3 mm a significantly increase (approximately 14%) of the resulted peak temperature is produced. On the other side, the welding speed showed a very small effect on the resulted heat, the change ratio could reach ± 2% only.

References

[1] R. S. Mishra and Z. Y. Ma, "Friction stir welding and processing," Materials Science and Engineering: R: Reports, vol. 50, no. 1, pp. 1–78, 2005. https://doi.org/10.1016/j.mser.2005.07.001.

[2] B. T. Gibson, D. H. Lammlein, T. J. Prater, W. R. Longhurst, C. D. Cox, M. C. Ballun, K. J. Dharmaraj, G. E. Cook, and a. M. Strauss, "Friction stir welding: Process, automation, and control," Journal of Manufacturing Processes, vol. 16, no. 1, pp. 56–73, Jan. 2014. https://doi.org/10.1016/j.jmapro.2013.04.002.

[3] Kim, Byeong-Jin, Hee-Seon Bang, and Han-Sur Bang. "The effect of tool profiles on mechanical properties of friction stir welded Al5052 T-Joints." Journal of Nanoscience and Nanotechnology, vol. 18, no. 3, pp. 1935-1939, 2018. https://doi.org/10.1166/jnn.2018.14995.

[4] L. Cui, X. Yang, Y. Xie, X. Hou, and Y. Song, "Process parameter influence on defects and tensile properties of friction stir welded T-joints on AA6061-T4 sheets," Materials and Design, vol. 51, pp. 161–174, 2013. https://doi.org/10.1016/j.matdes.2013.04.013.

[5] Y. Zhao, L. Zhou, Q. Wang, K. Yan, and J. Zou, "Defects and tensile properties of 6013 aluminum alloy T-joints by friction stir welding," JOURNAL OF MATERIALS&DESIGN, vol. 57, no. 2014, pp. 146–155, 2013.

[6] Y. Z. Li, Q. Z. Wang, B. L. Xiao, and Z. Y. Ma, "Effect of welding parameters and B4C contents on the microstructure and mechanical properties of friction stir welded B4C/6061Al joints," Journal of Materials Processing Technology, vol. 251, pp. 305–316, 2018. https://doi.org/10.1016/j.jmatprotec.2017.08.028.

[7] J. S. Jesus, J. M. Costa, A. Loureiro, and J. M. Ferreira, "Assessment of friction stir welding aluminium t-joints," Journal of Materials Processing Tech., vol. 255, no. 2010, pp. 387–399, 2018.

[8] D. K. P. PODRŽAJ, B. JERMAN, "Welding defects at friction stir welding," METALURGIJA, vol. 54, no. 2, pp. 387–389, 2015.

[9] Armansyah, I. P. Almanar, M. S. B. Shaari, M. S. Jaffarullah, N. Busu, M. A. F. Zainal, and M. A. A. Kasim, "Temperature distribution in friction stir welding using finite element method," International Journal of Mechanical and Mechatronics Engineering, vol. 8, no. 10, pp. 1699–1704, 2014.

[10] Y. R. Yatapu, B. R. Reddy, R. V. Ramaraju, M. Faizal, B. Che, and A. Bin Ibrahim, "Prediction of temperatures during friction stir welding of aa6061 aluminium alloy using hyperworks," ARPN Journal of Engineering and Applied Science, vol. 11, no. 18, pp. 11003–11008, 2016.

[11] D. M. Neto and P. Neto, "Numerical modeling of friction stir welding process : a literature review," International Journal of Advance Manufacturing Technology, vol. 65, pp. 115–126, 2013. https://doi.org/10.1007/s00170-012-4154-8.

[12] R. Nandan, G. G. Roy, and T. Debroy, "Numerical simulation of three-dimensional heat transfer and plastic flow during friction stir welding," Metallurgical and Materials Transactions A, vol. 37A, pp. 1247–1259, 2006. https://doi.org/10.1007/s11661-006-1076-9.

[13] M. S. Weglowski, "Friction stir processing – State of the art," Archives of Civil and Mechanical Engineering, vol. 18, pp. 114–129, 2018. https://doi.org/10.1016/j.acme.2017.06.002.

[14] HyperWorks Manufacturing Solutions, Altair Engineering, Inc.

[15] R. Nandan, T. Debroy, and H. Bhadeshia, "Recent advances in friction-stir welding – Process, weldment structure and properties," Progress in Materials Science, vol. 53, no. 6, pp. 980–1023, Aug. 2008. https://doi.org/10.1016/j.pmatsci.2008.05.001.

[16] D. Li, X. Yang, L. Cui, F. He, and H. Shen, "Effect of welding parameters on microstructure and mechanical properties of AA6061-T6 butt welded joints by stationary shoulder friction stir welding," vol. 64, no. 2014, pp. 251–260.

[17] X. He, F. Gu, and A. Ball, "A review of numerical analysis of friction stir welding," Progress in Materials Science, vol. 65, pp. 1–66, 2014. https://doi.org/10.1016/j.pmatsci.2014.03.003.

[18] H. J. Liu, J. C. Hou, and H. Guo, "Effect of welding speed on microstructure and mechanical properties of self-reacting friction stir welded 6061-T6 aluminum alloy," Materials and Design, vol. 50, pp. 872–878, 2013. https://doi.org/10.1016/j.matdes.2013.03.105.

[19] X. Hou, X. Yang, L. Cui, and G. Zhou, "Influences of joint geometry on defects and mechanical properties of friction stir welded AA6061-T4 T-joints," Materials and Design, vol. 53, no. 2014, pp. 106–117.

[20] L. Fratini, G. Buffa, and R. Shivpuri, "Influence of material characteristics on plastomechanics of the FSW process for T-joints," Materials and Design, vol. 30, no. 7, pp. 2435–2445. https://doi.org/10.1016/j.matdes.2008.10.014.